

ORIGINAL RESEARCH

Extending deep learning approaches for forest disturbance segmentation on very high-resolution satellite images

Dmitry E. Kislov¹ , Kirill A. Korznikov¹ , Jan Altman² , Anna S. Vozmishcheva^{1,3}  & Pavel V. Krestov¹ 

¹Botanical Garden Institute, Far Eastern Branch of the Russian Academy of Science, Makovskogo St. 142, Vladivostok 690024, Russia

²Institute of Botany, Czech Academy of Sciences, Pruhonice 25243, Czech Republic

³Siberian Federal University, Svobodny pr. 79, Krasnoyarsk 660041, Russia

Keywords

Bark beetle outbreak, DCNN, deep convolutional neural network, deep learning, forest damage detection, vegetation recognition

Correspondence

Kirill A. Korznikov, Botanical Garden Institute, Far Eastern Branch of the Russian Academy of Science, Makovskogo St. 142, 690024, Vladivostok, Russia. Tel: +7 423 2388041 106; Fax: +7 423 2388041; E-mail: korzir@mail.ru

Editor: Mat Disney

Associate Editor: Anna Cord

Received: 25 July 2020; Revised: 24 November 2020; Accepted: 4 December 2020

doi: 10.1002/rse2.194

Remote Sensing in Ecology and Conservation 2021; **7** (3):355–368

Abstract

Accurate remote detection of various forest disturbances is a challenge in global environmental monitoring. Addressing this issue is crucial for forest health assessment, planning salvage logging operations, modeling stand dynamics, and estimating forest carbon stocks and uptake. Substantial progress on this problem has been achieved owing to the rapid development of remote sensing devices that provide very high-resolution images. Concurrently, image processing algorithms have witnessed rapid development owing to the extensive use of artificial neural networks with complex architectures and deep learning approaches. This opens new opportunities and perspectives for applying deep learning methods to solving various problems in environmental sciences. In this study, we used deep convolutional neural networks (DCNNs) to recognize forest damage induced by windthrows and bark beetles. We used satellite imagery of very high resolution in visual spectra represented as pansharpened images (RGB channels). When predicting forest damage, we obtained accuracies higher than 90% on test data for recognition of both windthrow areas and damaged trees impacted by bark beetles. A comparative analysis indicated that the DCNN-based approach outperforms traditional pixel-based classification methods (AdaBoost, random forest, support vector machine, quadratic discrimination) by at least several percentage points. DCNNs can learn a specific pattern of the area of interest and thus yield fewer false positive decisions than pixel-based algorithms. The ability of DCNNs to generalize makes them a good tool for delineating smooth and ill-defined boundaries of damaged forest areas, such as windthrow patches.

Introduction

Forests are principal controllers of various processes on a global scale. They provide many ecosystem services, including carbon balance in the Earth's atmosphere (Dixon et al, 1994) and indispensable repositories for terrestrial biodiversity (Liang et al, 2016). The high importance of forests for natural systems and human society explains the attention of environmental organizations and forest management services to ongoing forest area reduction due to anthropogenic pressure or natural disturbance processes.

It has been documented that global climate change can increase the severity of forest damage events (Dale et al,

2001; Millar & Stephenson, 2015; Seidl et al, 2017). Increases in natural disturbances in forests due to global climate change have stimulated the development of more precise methods for recognition damaged forest areas (Sommerfeld et al, 2018). This makes the development and application of methods for detecting windthrow patches of high interest in view of forest management goals, such as the organization of salvage logging, carbon balance, and fire risk assessments (Quine et al, 1995).

To date, an impressive arsenal of methods for monitoring forest cover dynamics using remote sensing data have been developed. These include successfully implemented and widely used algorithms for recognizing forest damage

based on multispectral satellite imagery distributed in time MODIS (Sulla-Menashe et al, 2014), Landsat (Potapov et al, 2020; Senf et al, 2017), and Sentinel-2 (Abdullah et al, 2019).

Another approach is based on one-time, very high-resolution (VHR) snapshots from satellite systems and/or unmanned aerial vehicles (UAVs) and combining these data with ground-based studies (Hamdi et al, 2019; Safonova et al, 2019). This approach allowed us to improve existing techniques for observing forest cover and has become widely used due to an increase in the number of satellite or UAV systems providing VHR images (<1 m/pixel). Images of VHR provide the ability to precisely delineate the boundaries of tree crowns and damaged forest sites (Einzmann et al, 2017).

Different types of forest damage can be easily recognized by VHR imagery. Patterns characterized by fallen tree trunks are specific for forest sites damaged by strong winds (Hamdi et al, 2019; Kislov & Korznikov, 2020). Damage caused by other prolonged disturbance agents (e.g., insects, fungi, droughts, and floods) can be characterized by gradually changing the crown color from green to brown and finally gray (Dennison et al, 2010). Insect outbreaks are usually prolonged events, and impacted trees are subjected to different stages of damage, exhibiting partially yellowed crowns to completely gray crowns for dead trees (Safonova et al, 2019). All damage sources can be recognized by physiological characteristics (Junttila et al, 2019) and changes in vegetation index scores (Olsson et al, 2016).

The problem of recognizing forest disturbances on satellite imagery is a formally image segmentation problem. In this context, the problem consists of partitioning the whole image into multiple segments or objects that coincide with damaged or non-damaged forest areas. Segmentation plays a central role in a broad range of applications in environmental sciences (Yuan et al, 2020) and is a challenging problem in computer vision (Minaee et al, 2020). To date, many image segmentation algorithms have been developed. These include methods such as *K*-means clustering (Dhanachandra et al, 2015), thresholding (Otsu, 1979), region-expanding (Nock & Nielsen, 2004), and advanced algorithms, including conditional and Markov random fields (Plath et al, 2009), graph cuts (Boykov et al, 2001), sparsity-based methods (Starck et al, 2005), and active contours (Kass et al, 1988).

As the origin of many state-of-the-art image processing techniques and showing extraordinary results in image segmentation problems, deep learning (DL) has become increasingly popular for vegetation mapping (Mazza et al., 2019; Wagner et al, 2019), recognizing damaged forest sites on satellite imageries (Sylvain et al, 2019) and applications in various fields related to the processing of

remote sensing data (Ma et al, 2019; Paoletti et al, 2019). Over the past few years, a new generation of image segmentation algorithms has emerged on the basis of the DL concept. These algorithms rely on the construction of neural networks with many hidden layers and are generically referred to as DL models (Chen et al., 2017; Krizhevsky et al, 2017). Land cover mapping and automatic detection of forest disturbances by satellite imagery from high- to VHR as a particular area comprise the fields where DL is intensively used and showed its potential (Kattenborn et al, 2019).

In this study, we demonstrated the use of DL in segmentation of damaged forest sites by pansharpened RGB (red, green, blue) VHR satellite imagery. As an example, we considered two types of natural disturbances in southern taiga forests: windthrows and individual tree dried due to insect damage. It is worth noting that the ability to handle multiple resolutions is a crucial point when processing remote sensing data (Mesner & Oštr, 2014). In the field of DL and image processing, there are a lot of studies aimed at discovering influence of imagery resolution on segmentation accuracy (Duarte et al, 2018). However, there is a lack of studies related to assessment of the spatial resolution effect on the recognition of forest disturbances using DL methods.

Another important point to be considered is how DL segmentation algorithms outperform traditional machine learning (ML) methods. Comparison studies between DL and standard ML methods followed by applying specific feature engineering techniques, such as histogram of gradients (HOG) and grey level co-occurrence matrices (GLCM) are not new (Alhindi et al, 2018). There are many applied problems that can be solved by traditional ML algorithms and having accuracy scores comparable to those obtained by DL approaches (Lee et al, 2019). However, there are blank spaces in research related to the problem of recognizing forest disturbances, especially those connected to employing pansharpened RGB satellite imagery.

Materials and Methods

Study sites

The study area consist of two sites located in Kunashir and Sakhalin islands, Russia (Fig. 1). Non-disturbed forests are natural in the study sites represented by dark coniferous forests dominated by Sakhalin fir *Abies sachalinensis*, Yezo spruce *Picea jezoensis*, and Sakhalin spruce *Picea glehnii* as well as rare inclusions of Japanese yew *Taxus cuspidata* and Dahurian larch *Larix gmelinii*. These southern taiga forests are characterized by the presence of many broad-leaved species. Ferns and dwarf bamboos (*Sasa* spp.) are common under the canopy layer. The

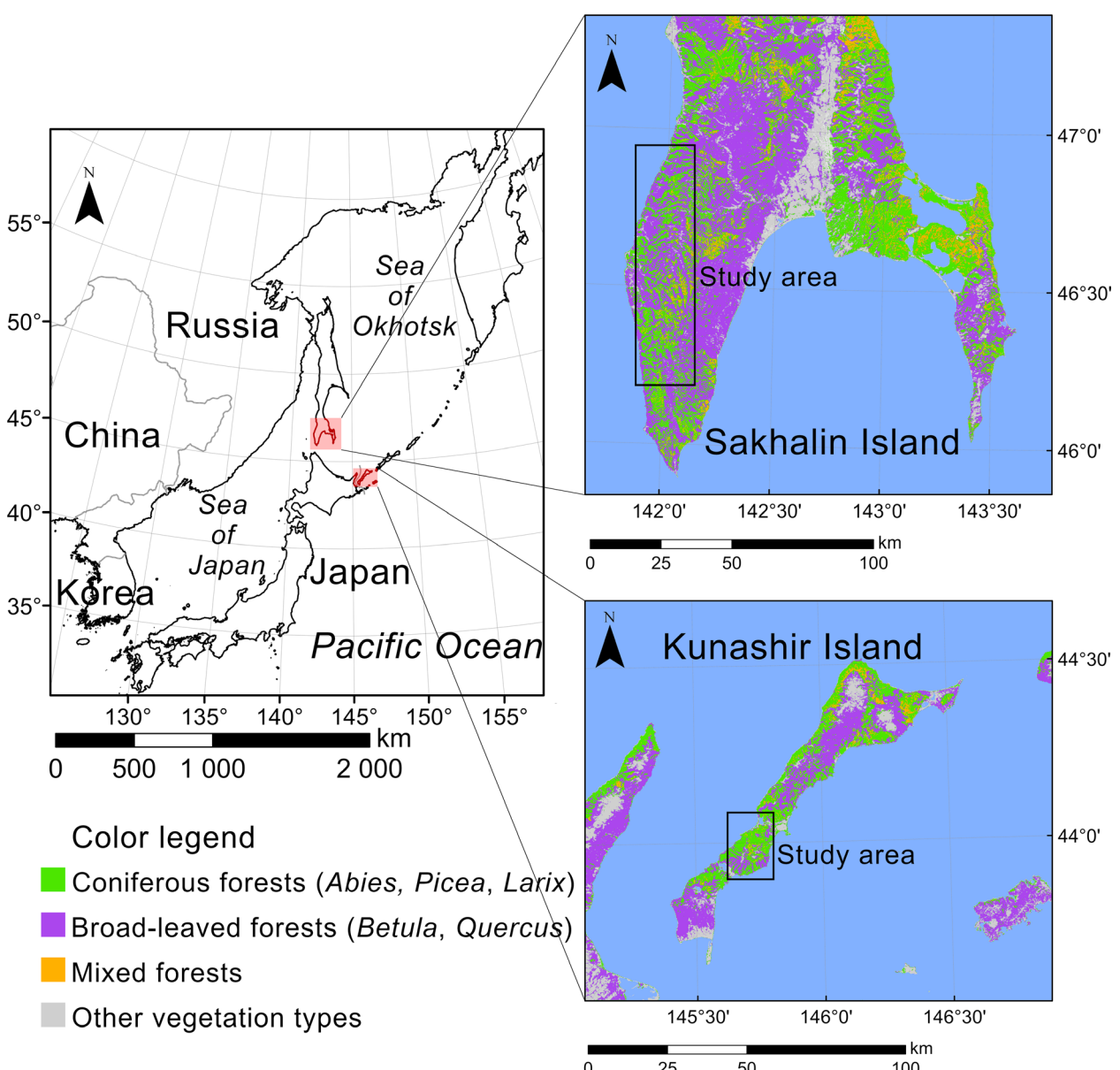


Figure 1. Study areas.

average height of the stands is 17–18 m, and the total volume of stem wood is estimated as $150\text{--}180 \text{ m}^3 \cdot \text{ha}^{-1}$ (Vlasov, 1959).

In the 2010s, forests in this region were affected by several strong wind disturbances. In October 2015, Sakhalin Island suffered two catastrophic cyclones which led to the appearance of large windthrow patches. It has been documented that disturbance activity in our study area, northeast Asia, is increasing as tropical cyclones are moving poleward and increase their intensity (Altman et al, 2018; Webster et al, 2005). In December 2014, strong winds were accompanied by the sticking of wet snow on tree crowns on

Kunashir Island. Massive windfalls precipitated the rapid growth of bark beetle (*Ips typographus japonicus*) populations, which prefer spruce trees; thus, pest damage to firs was less intensive. We consider the simultaneous appearance of drying trees as an event that is likely caused by bark beetle outbreaks (de Groot et al, 2018; Havašová et al, 2017). However, it is impossible to separate dried trees due to bark beetle attacks and trees drying because of other potential disturbance agents without ground-based research. In this study, to avoid such crucial issues and ensure the correctness of delineated forest disturbance sites, we used fieldwork data collected from 2018–2019.

Deep learning methods

To date, more than one hundred deep neural network algorithms have been developed to solve instance and semantic segmentation problems (Minaee et al, 2020). One efficient encoder–decoder network architecture used for image segmentation is U-Net. Originally, U-Net was proposed by Ronneberger et al (2015) for segmenting biological microscopy images. Since then, various U-Net-like CNNs have been developed for different types of image segmentation problems.

In this study, we used a deep neural network of encoder–decoder type that was built on top of U-Net (Fig. 2). We extended the standard block of U-Net by including additional residual and batch normalization layers. The inclusion of these layers is controlled by special Boolean parameters, which allowed us to investigate different U-Net-like architectures by changing these parameters. Another extension of the U-Net was based on a depth parameter of the encoder and decoder paths. This yielded the deep convolutional neural network (DCNN), which we refer to as a U-Net-like CNN, that became highly efficient for segmenting windthrow patches in VHR satellite imagery (Hamdi et al, 2019; Kislov & Korznikov, 2020).

Based on the results of a previous study, we started with the model presented in (Kislov & Korznikov, 2020) with the following set of parameters, which are given in the form “parameter = value”: the number of output channels (`out_ch = 1`); initial number of filters (`start_ch = 64`); depth of the model (default value for U-Net is 4, `depth = 4`); incremental rate (`inc_rate = 2`), which describes how the number of filters change when we step-down through the network architecture (default number of filters for U-Net presented by the following sequence: 64, 128, 256, 512, 1024); activation function (`activation = “relu”`); dropout rate (`dropout = 0.5`); is

batch normalization turned on in conv/up-conv blocks? (`batchnorm = True`); is max-pooling used in blocks? (`maxpool = True`); what strategy of upsampling is used? (`upconv = True`); and are there additional concatenations within conv-blocks of the U-Net like model? (`residual = false`).

Data source and preparation

We used VHR satellite imagery for specific areas, which are highlighted on the map in Figure 1 by red squares. These images were provided as pansharpened RGB snapshots (Tables 1 and 2; Fig. 3). The delineation of forest disturbance areas was performed manually.

Neural network training

Considering the essence of DL compared to pixel-based methods of imagery segmentation, we should provide images with sufficient resolution for training and validation. Because DL algorithms are able to understand specific patterns of the object or region to be recognized, the images that are used for training and validation should be sufficient should be sufficient in size to contain that specificity. In the case of the windthrow detection problem, it is sufficient to use images that cover several tens of meters, as this is usually enough to recognize fallen stems on images. For pansharpened satellite imagery with a resolution of 0.3–0.6. meter/pixel, it is usually sufficient to take 256×256 images (Kislov & Korznikov, 2020).

In this study, training and validation data were generated as batches of size (m , 256, 256, 3). For training, we internally implemented a stream (Python generator) of overlapped sub-images that were randomly cropped from the original satellite images. Finally, these sub-images were combined into batches and used for neural network

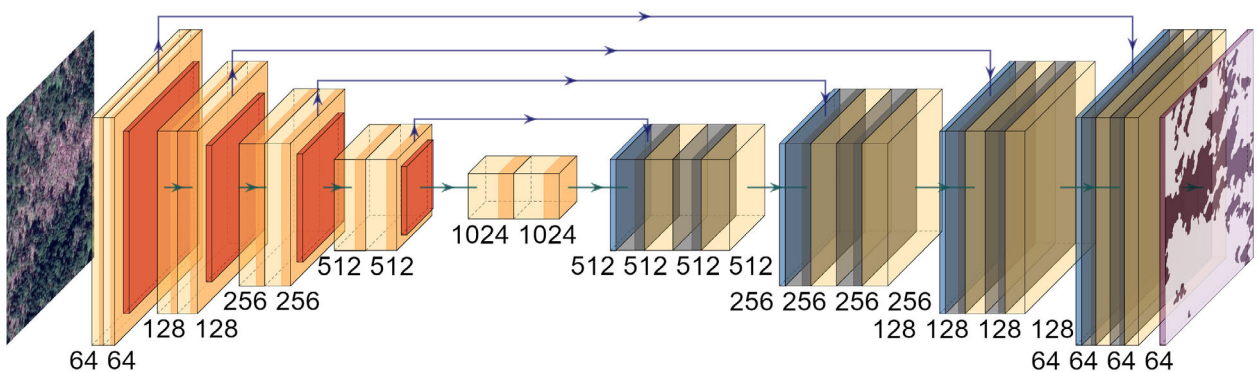


Figure 2. U-Net-like CNN architecture; in contrast with the original U-Net, it includes batch normalization after each convolutional and dropout layer after the first pair conv + batch norm within each encoding block. The figure was generated using PlotNeuralNet library (<https://github.com/Harislqbal88/PlotNeuralNet>).

Table 1. Images used for training, validation, and testing of the U-Net-like CNN.

Image name; size (pixels); central coordinates; main objects	Image preview
train1 2560 × 2560 43.9889° N 145.6733° E coniferous and mixed forests: damaged and healthy trees; forest clearings	
train2 2560 × 2560 44.0197° N 145.6818° E coniferous and mixed forests: damaged and healthy trees; forest clearings; sea surface; seashore	
train3 1280 × 1280 44.0024° N 145.7073° E coniferous and mixed forests: damaged and healthy trees; forest clearings; dwarf bamboo thickets; road	
train4 960 × 480 43.9980° N 145.6988° E coniferous and mixed forests: damaged and healthy trees; mining pit, road; forest clearings	

(Continued)

training. Therefore, each training iteration required m images to be streamed and composed in the batch. If the entire training process requires k iterations, this leads to the generation of $m \times k$ sub-images. Validation data

Table 1. Continued.

Image name; size (pixels); central coordinates; main objects	Image preview
validation1 1280 × 1280 43.9224° N 145.6743° E coniferous and mixed forests: damaged and healthy trees; dwarf bamboo thickets; forest clearings; road; eroded surfaces	
test1 2560 × 2560 43.9887° N 145.6898° E coniferous and mixed forests: damaged and healthy trees; forest clearings; dwarf bamboo thickets; road	
test2 960 × 480 43.9961° N 145.6988° E coniferous and mixed forests: damaged and healthy trees; mining pit, road; forest clearings	

The problem of recognizing damaged trees by bark beetles is illustrated. Digital Globe Worldview-2 satellite system, 11 September 2018, ID 1030010084511200, nadir 30.8°, sun elevation 48.4°, max ground sample distance 0.62 m.

were generated in the same manner from a separate set of satellite images (Tables 1 and 2), ensuring that image tiles do not overlap. Validation images were used during neural network training. The test data were obtained from a set of new satellite images that were not included in either the training or validation datasets.

Another important part of the neural network training process is augmentation. Augmentation reduces the risk of overfitting (Chollet, 2015; Shorten & Khoshgoftaar, 2019) and allows for the number of images used during the training process to be significantly expanded. The logic behind the augmentation can be illustrated by the example of the windthrow patch identification problem:

Table 2. Images used for training, validation and testing U-Net-like CNN¹.

Image name; size (pixels); central coordinates; main objects	Image preview
train1 2560 × 2560 46.4368° N 142.0003° E windthrows; coniferous and mixed forests; dwarf bamboo thickets	
validation1 2560 × 2560 46.4577° N 142.0885° E windthrows; coniferous and mixed forests; dwarf bamboo thickets	
test1 1280 × 1280 46.4474° N 142.0036° E windthrows; coniferous and mixed forests; dwarf bamboo thickets	

The problem of windthrow patch recognition is illustrated. Digital Globe Worldview-3 satellite system, 5 September 2017, ID 104001003372A300, nadir 28.9°, sun elevation 49.1°, max ground sample distance 0.39 m.

¹The Pretrained U-Net CNN was developed using snapshots from Airbus Pleiades-1A/B images with spatial resolution 0.5 m/pixel; for details, see supplementary materials in Kislov and Korznikov (2020).

windthrow patches are invariant to image rotations; thus, we can use original images and slightly rotated ones during the network training process. It is worth noting that augmentation is a problem-specific procedure that can consist of various image transformations, including color adjustment, zooming, and random shifts.

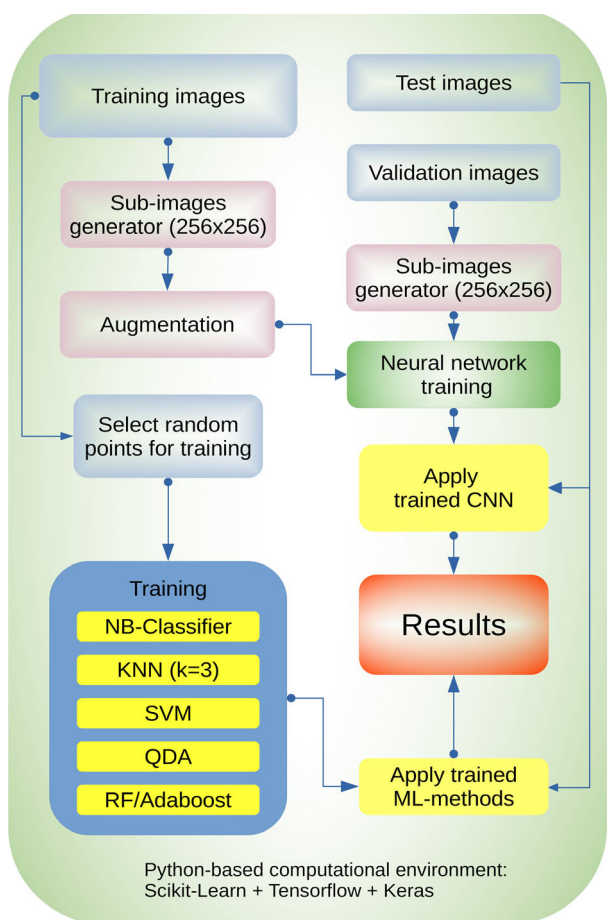


Figure 3. DCNN training and algorithm comparison workflow.

In the case of the windthrow identification problem, we chose random changes of RGB channels of the original images and random vertical and horizontal flips. Random changes for each RGB channel did not exceed 0.1 by absolute value and were applied simultaneously to all channels, as it is implemented in the utility function “apply channel shift” from the Keras package (Chollet, 2015). Random flips provided additional variability of images used for training and reduced overfitting. We also considered using small random rotations in the augmentation pipeline. However, adding rotations did not improve the network performance, and we excluded such transformations from the augmentation. Therefore, with a batch size of 20 and performing typically up to 1500 iterations for training the network, we streamed up to 30 000 different augmented 256 × 256 images.

The augmentation pipeline used for the problem of recognizing trees damaged by bark beetles was almost the same as that of windthrow segmentation, except that changes in RGB channels were omitted. We did not use random shifts in the augmentation pipeline. Such

transformations would be redundant because sub-images were cropped out from a fixed set of satellite images and often intersected each other that could be considered as they are spatially shifted.

A generic workflow diagram for the neural network training is shown in Figure 3.

Neural network training was performed by Adam (Kingma & Ba, 2014) as an optimization algorithm, and binary cross-entropy was performed as a loss function. This method is widely used when dealing with image segmentation and binary classification problems (Mannor et al, 2005). Along with the binary cross-entropy loss function, we considered losses that focus on imbalanced segmentation. These were balanced cross-entropy (BCE) and Dice loss function. The windthrow segmentation and recognition of trees damaged by bark beetles problems had different degrees of class imbalance and therefore yielded slightly different recommendations regarding loss function choice. However, bearing in mind that the model being trained with the default (binary cross-entropy) loss function is able to learn and give accurate results, we decided to use the default loss function.

We attempted different values of the learning rate parameter starting from $1.0e^{-2}$ to $1.0e^{-5}$. The former led us to relevant fluctuations of the loss function, the latter yielded in increasing the number of iterations required for the network training. Finally, we decided to go with a learning rate value equal to $1.0e^{-4}$, which is closer to its default value and does not lead to significant fluctuations in the loss function.

We considered different approaches as stopping criteria during neural network training. These include setting up the number of iterations and tracking dynamically evaluated metric values on validation data. The latter approach became more progressive and allowed for the prevention of the CNN overfitting phenomenon (when the CNN performs significantly worse on the validation data and better on the training data). We stopped the training process when the performance metrics began increasing for the training data and decreasing for the test data. When that happens, the model begins to learn very specific patterns (overfits) of the training dataset and loses the ability to generalize.

In the case of the windthrow detection problem, we considered two models (below addressed as U-Net-like CNN and U-NetR CNN) trained on images of different resolutions. The first was originally trained on the image set used in our previous work (Kislov & Korznikov, 2020) and had a resolution of 0.5 m/pixel. However, this network produced worse results with higher resolution images (0.3 m/pixel with a maximum ground sample distance of 0.39 m), and we retrained it. Therefore, the U-NetR CNN is a retrained version of U-Net-like CNN on

an extended set of images. The retraining procedure consisted of using the U-Net-like CNN model and further training it on the extended image set presented in Table 2 and those used in our previous work.

All computations were performed on a PC with 1 GPU Nvidia Tesla K80 with 16 GB of RAM and required up to 10 h to train the neural network.

Comparison with standard machine learning methods

In contrast with DCNNs, traditional ML methods (without applying specific feature extraction algorithms such as HOG-features (McConnell, 1986) or GLCM features (Haralick et al, 1973) do not account for neighboring pixels relative to the pixel being classified at a given moment. As we could expect, such methods should have lower performance than those that consider neighboring pixels.

For comparison, we utilized commonly used ML algorithms: the naive Bayes classifier (Zhang, 2004), quadratic discriminant analysis (Huberty, 1975), support vector machine (Cortes & Vapnik, 1995), Random Forest classifier (Breiman, 2001), and AdaBoost classifier (Freund & Schapire, 1997). We used the default implementation of these algorithms, as given in the Scikit-Learn package (Pedregosa et al, 2011). All these methods were trained on a randomly chosen subset of 600 000 points.

Another option for improving segmentation accuracy for shallow ML methods is to conduct the feature engineering step before applying these algorithms. To date,

Table 3. Comparison of U-Net-like CNN and standard ML methods for Detection of trees damaged by bark beetles.

Algorithm	BA/threshold	F1/threshold	IoU/threshold
Images with forested area with trees damaged by bark beetles			
AB	0.97/0.48	0.87/0.50	0.77/0.50
KNN	0.95/0.01	0.85/0.34	0.74/0.34
NB	0.87/0.08	0.63/0.93	0.46/0.93
QDA	0.97/0.05	0.87/0.95	0.77/0.95
RF	0.96/0.03	0.86/0.42	0.76/0.42
SVM	0.95/0.01	0.85/0.34	0.74/0.34
U-Net-like CNN	0.97/0.07	0.79/0.28	0.65/0.28
Images with patterns lead to false-positive cases (road, open pit)			
AB	0.92/0.48	0.50/0.50	0.33/0.50
KNN	0.88/0.01	0.59/0.34	0.42/0.34
NB	0.85/0.04	0.40/0.38	0.25/0.38
QDA	0.92/0.01	0.52/0.01	0.30/0.08
RF	0.89/0.08	0.55/0.35	0.38/0.35
SVM	0.92/0.04	0.48/0.09	0.32/0.09
U-Net-like CNN	0.94/0.48	0.62/0.51	0.45/0.51

Algorithm abbreviations: AB, AdaBoost; KNN, K-nearest neighbor ($k = 3$); NB, Naive Bayes; QDA, Quadratic Discriminant Analysis; RF, Random Forest; SVM, Support Vector Machine.

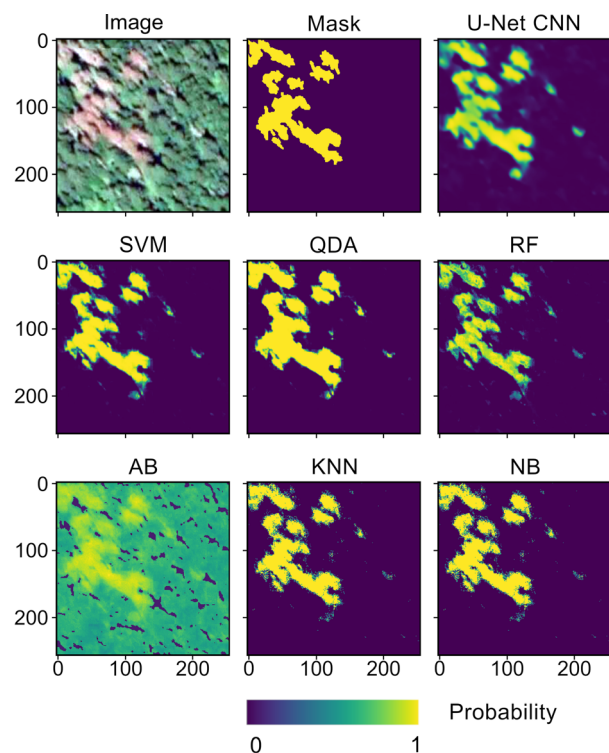


Figure 4. Forest damages caused by bark beetles: algorithm comparison. Algorithm abbreviations: AB, AdaBoost; KNN, K -nearest neighbor ($k = 3$); NB, Naive Bayes; RF, Random Forest; QDA, Quadratic Discriminant Analysis; SVM, Support Vector Machine.

many texture features have been proposed (Humeau-Heurtier, 2019). It is a tremendously complex problem to choose an appropriate set of features that will be relevant for each particular classification or segmentation problem. In our case, we conducted several computational experiments to demonstrate the potential of shallow ML methods with basic texture-specific features. For each pixel of an image, we computed two texture-specific features based on the concept of a grey-level co-occurrence matrix (GLCM). We used default (as presented in the documentation of Scikit-learn (https://scikit-image.org/docs/dev/auto_examples/features_detection/plot_glcm.html)) parameters (distance = [5 pixels], angles = [0 degrees]) to compute GLCM and calculated “dissimilarity” (DIS) and “correlation” (CORR) features (<https://scikit-image.org/docs/dev/api/skimage.feature.html#skimage.feature.greycoprops>). The patch size for which GLCMs were calculated was 10 pixels in size and the pixel of interest was assumed to be at the center of this patch (edge case issues were excluded by means of padding with (patch size)/2). These features were consequently used to train traditional ML algorithms. We considered two sets of features: (R, G, B, DIS) and (R, G, B, DIS, and CORR).

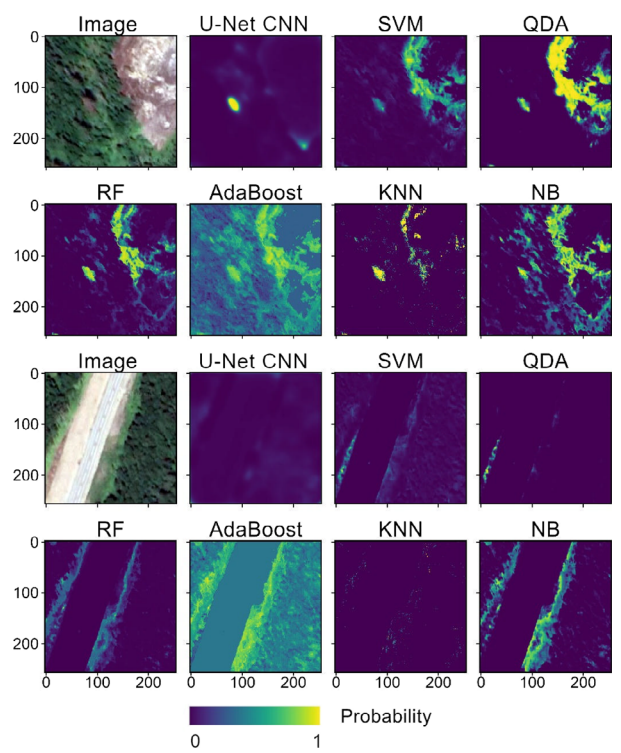


Figure 5. Forest damages caused by bark beetles: false-positive cases. Algorithm abbreviations: AB, AdaBoost; KNN, K -nearest neighbor ($k = 3$); NB, Naive Bayes; RF, Random Forest; QDA, Quadratic Discriminant Analysis; SVM, Support Vector Machine.

Validation approach

To assess the accuracy of the proposed algorithms for the windthrow detection problem, we considered several score functions that are commonly used in DL: 1) balanced accuracy score (BA), 2) F1 score, and 3) intersection over union (IoU) or Jaccard index. The latter is widely used for performance assessment in semantic segmentation problems (Rezatofighi et al., 2019).

Each score function requires two arguments to be passed to compute its value. These are exact (true) and predicted values. In the case of semantic segmentation, these arguments are presented by two images; the former is exactly the mask of test images (e.g., 0 for background pixels and 1 for pixels belonging to the area of interest), and the latter is the prediction obtained by the image segmentation algorithm. Owing to the internal implementation of most image segmentation algorithms, it is possible to interpret their outputs as probabilities of a pixel belonging to the segmented area. This approach provides a common strategy for turning a map of probabilities into a binary mask by specifying a threshold value. If the probability value in the current pixel is greater than the

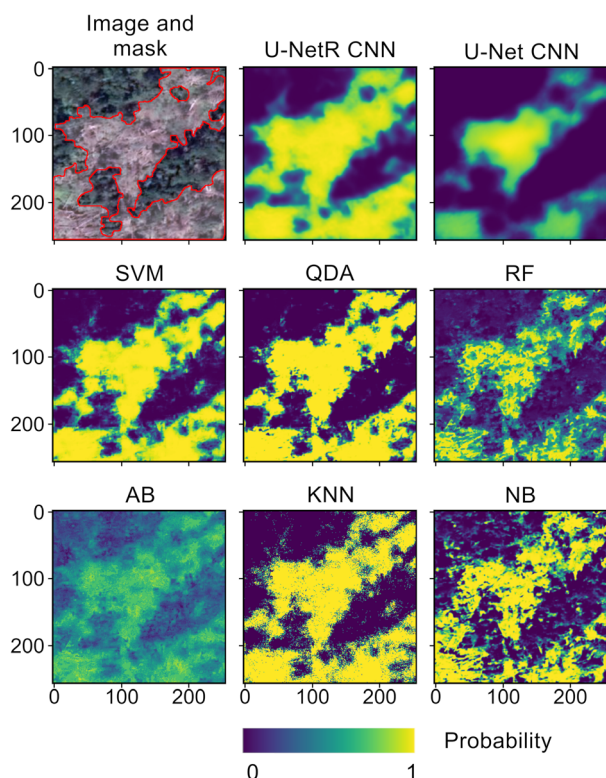


Figure 6. Windthrow segmentation: algorithm comparison. Algorithm abbreviations: AB, AdaBoost; KNN, K -nearest neighbor ($k = 3$); NB, Naive Bayes; RF, Random Forest; QDA, Quadratic Discriminant Analysis; SVM, Support Vector Machine; U-NetR CNN, Retrained U-Net-like CNN.

threshold, the pixel is assumed to belong to the area of interest; otherwise, it is not. Thus, the problem of finding the optimal value of the threshold can be formulated for each combination of a particular algorithm and score metric.

Results and Discussion

Bark beetle outbreaks detection

The results shown in Table 3 and Figure 4 demonstrate that the U-Net-like CNN provides almost the same accuracy of identification of damaged trees as traditional pixel-based algorithms, except for the naive Bayes algorithm. Algorithms such as SVM and QDA lead to even better results than U-Net-like CNN because of the precise separation of pixels lying in the vicinity of the boundaries of damaged forest areas. These results remain valid for relatively homogeneous forest stands, without inclusion areas of the same color composition as damaged tree crowns. However, when the study sites have optical properties similar to damaged tree crowns (e.g.,

Table 4. Comparison of U-Net-like CNN and standard ML methods. Windthrow detection problem.

Algorithm	BA/ threshold	F1/ threshold	IoU/ threshold
AB	0.86/0.51	0.86/0.50	0.76/0.50
KNN	0.85/0.67	0.85/0.67	0.75/0.34
NB	0.77/0.68	0.79/0.47	0.65/0.47
QDA	0.88/0.84	0.88/0.75	0.78/0.75
RF	0.86/0.77	0.86/0.73	0.76/0.73
SVM	0.88/0.67	0.88/0.59	0.79/0.59
U-Net-like CNN	0.90/0.02	0.90/0.01	0.80/0.01
Retrained U-Net-like CNN	0.92/0.48	0.92/0.50	0.81/0.50

Algorithm abbreviations: AB, AdaBoost; KNN, K -nearest neighbor ($k = 3$); NB, Naive Bayes; QDA, Quadratic Discriminant Analysis; RF, Random Forest; SVM, Support Vector Machine.

eroded near-road slopes, exposed lands, open pits, etc.), pixel-based methods are subjected to significant accuracy degradation due to an increase in false-positive pixel classification.

Based on the results presented in Figure 5, we concluded that the U-Net-like CNN does not lead to pixel misclassifications in the vicinity of the road but has false positive decisions for a small area at the bottom of the open pit. The latter phenomena are caused by the similarity of the damaged forest pattern and the context, the exposed land surrounded by green trees. Thus, if the source of errors is pattern-specific, a U-Net-like CNN is suitable and can likely achieve better scores than pixel-based methods.

Windthrows detection problem

In contrast with trees damaged by bark beetles, windthrow patches on pansharpened satellite images exhibit specific patterns. Earlier, we demonstrated good efficacy of using a U-Net-like CNN for recognition of windthrow areas in southern taiga forests (Kunashir Island, Russia). In this study, we used a neural network of the same architecture trained on previous data (Kislov & Korznikov, 2020) and applied it to images of slightly different resolutions and belonging to Sakhalin Island.

For comparison, we considered two U-Net-like CNNs (Fig. 6). The first was trained on images from Kunashir Island (denoted as U-Net-like CNN) with a resolution of 0.5 meter/pixel (Pleiades-1) and the second (denoted as Retrained U-Net-like CNN) was trained on an enriched set of satellite images, which include satellite imagery of 0.3 meter/pixel resolution (WorldView-3) from Sakhalin Island. The computed accuracy metrics for the windthrow recognition problem along with the corresponding

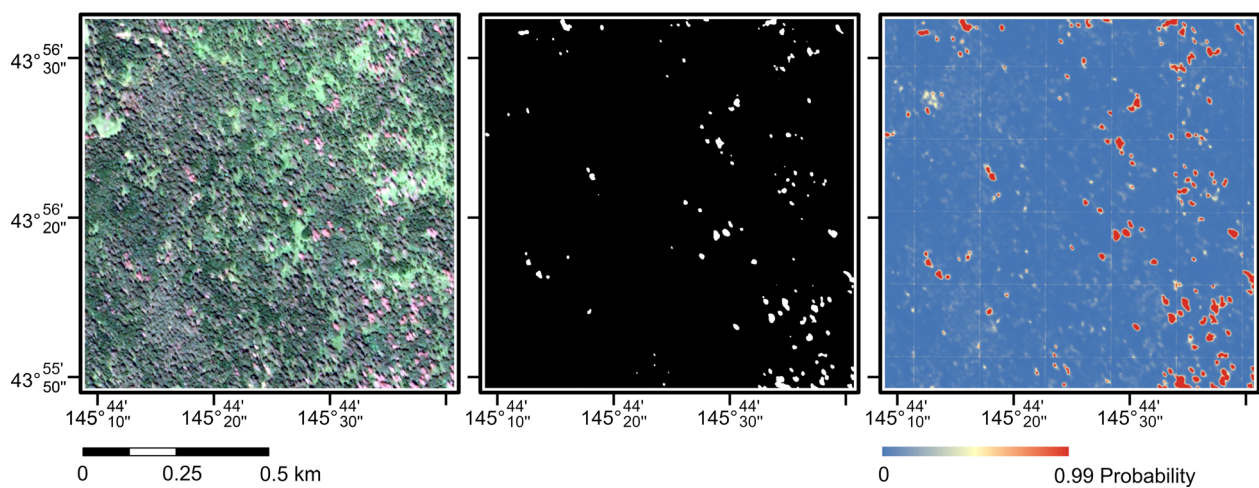


Figure 7. Example of forest damage assessment in bark beetle outbreak on 1 km² area using U-Net-like CNN, Kunashir Island.

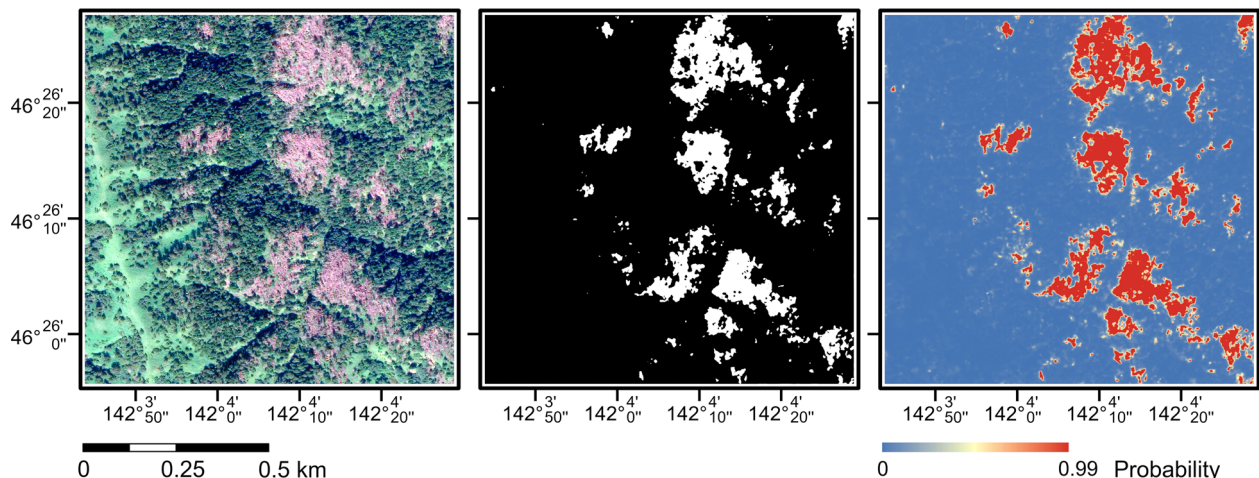


Figure 8. Example of windthrow patches assessment on 1 km² area using the Retrained U-Net-like CNN, Sakhalin Island.

optimal threshold values (maximizing the score function vs. threshold) are given in Table 4.

As expected, the U-Net-like CNN trained on low-resolution images (0.5 meter/pixel) and being applied to images of higher resolution (0.3 meter/pixel) leads to underestimation of the windthrow areas and precision loss. Because of the deep nature of the neural network, it became possible to retrain it on an enriched set of images (including VHR images for Sakhalin Island) and learned it to understand windthrow patches on images of both resolutions. We suspect that similar behavior can be achieved by inclusion of zoom transformation in the augmentation pipeline. However, using images of higher resolution provides more details about windthrow patterns and therefore should be preferred over artificial zooming.

Comparison with feature engineering techniques

Finally, we computed score metrics for two sets of features: (R, G, B, DIS) and (R, G, B, DIS, CORR) (similar to those presented in Tables 3 and 4) and found that in general, there was a tendency to improve segmentation accuracy when we were consequently moving from (R, G, B) to (R, G, B, DIS, CORR) feature set.

For the SVM in Table 4, we obtained 0.79241 for the (R, G, B) feature set (this rounded value is given in Table 4), 0.794 for (R, G, B, DIS), and 0.799 for (R, G, B, DIS, CORR). Other ML methods, such as NB and RF, also showed improvement in segmentation accuracy when using the extended feature set (R, G, B, DIS, and CORR), but these improvements were still not significant

(maximal increase of accuracy metric (any metric of BA, IoU, and F1) was not greater 0.08). Therefore, we might suppose that an appropriate choice of texture-specific features could improve segmentation accuracy and make it comparable to those obtained by some DL methods (at least for considered applied problems), but it requires a lot of feature engineering studies to be done.

Advantage of DCNNs

The use of the DL approach has some advantages: (1) once trained, neural networks are performant and able to process many pixels at a time; (2) they are able to remember complex patterns and usually lead to better results than pixel-based algorithms; (3) in comparison to most efficient standard ML methods, neural networks can train on a huge number of data (e.g., training support vector machines requiring significant computational time if the number of points in the training dataset is greater than 1 M) (Moré, 1978); and (4) an appropriate choice of texture-specific features could improve segmentation accuracy of standard ML methods, but this requires significant feature engineering work. DL models are free from such issues and can extract relevant features internally without feature engineering studies, which usually requires additional time and labor from the researcher.

Problem of a manual delineation approach

Training and validation processes require precise masks of target regions on images. These masks are usually delineated manually by a human and used to train the neural network to recognize the desired area and estimate its accuracy. However, delineation of some patterns, such as windthrow patches, can be very tricky due to their ambiguity. Windthrow patches have a complicated and spatially distributed structure, and it is difficult to put a line that deterministically separates a windthrow patch from a non-windthrow area. Making a delineation, an expert could not be completely sure that the line they drew restricted the desired area in an optimal way. There might be standalone alive trees among the fallen ones, or vice-versa, a few fallen trees within alive stands. In other words, it is not a problem to identify the area of interest in an image, but it might be difficult to outline this area correctly. If the area of interest is of complex structure, one can even make a mistake in the delineation step, for example, some areas of interest could be misdelineated or missed. Being a part of the training dataset, such errors may lead to accuracy degradation for trained neural networks. However, if the total area of correctly delineated regions significantly larger the cumulative area of mistakenly delineated regions, the neural network can be learned to generalize and recognize the desired patterns.

Nevertheless, inaccuracies in visually delineated data imply that the model applied to that data might perform better than the reference mask. Our results confirm the conclusions of Kattenborn et al (2019, 2020) because CNNs are able to overcome barriers and biases resulting from inaccessible sites.

Thus, accurate mask delineation significantly reduces possible biases at the validation and test stages of algorithms. This, in turn, implies additional requirements for the skill of a person performing visual delineation of target regions and objects. Moreover, as it yields from our experience, field-based studies could significantly improve the quality of visual delineation of satellite imagery. In contrast with pixel-based algorithms, in which decisions depend on pixel properties, the CNN-based approach works smoothly near segmented patterns. This leads to a gradient-like distribution of probabilities in the vicinity of the target area borders. Such decisions are similar to expert-based solutions. From an expert point of view, it is easier to outline a band that likely would include the separation curve, rather than to draw that curve exactly. Finally, to obtain a binary segmentation map (Figs. 7 and 8), one should apply a cut-off to probabilities using a threshold. Optimal threshold values for different score metrics are given in Tables 3 and 4.

It should be noted that the area of applying the trained U-Net-like CNN model and its performance depend on the set of images used for training. There could be various ground-based objects with similar patterns as objects of interest, and it could be almost impossible (even for expert-based segmentation) to avoid false-positive decisions without attracting fieldwork data. As it follows from our computational experiments, it is highly desirable to train the model on images that are close (made in similar conditions as possible) to those where the model is planned to be applied to. However, this restriction is not as crucial as it could be seen at first. The deep learning methods generally work well, and their accuracy can be characterized as almost not inferior to a human eye.

Conclusion

In this study, we demonstrated that the proposed DL algorithm (U-Net-like CNN) is an efficient method of automatically recognizing forest sites disturbed by winds and bark beetles. If appropriately trained, a U-Net-like CNN can identify specific types of damaged forests and their locations. In contrast with standard ML methods, DL algorithms do not require complex feature engineering. They are able to discover pattern-specific features internally and yield good recognition results with images of different resolutions and captured in slightly different conditions. The main advantage of DCNN is the ability

to understand the surrounding context of areas of interest. In the case of the dried tree identification problem, open and eroded road slopes could be a source of false-positive decisions because they might have patterns similar to dried tree crowns. The use of DCNN algorithms in such cases reduces the number of incorrectly segmented pixels owing to the ability to learn the surrounding context.

Acknowledgements

K.K. and D.K. research was funded by the Russian Science Foundation, grant number 20-74-00001. A.V. was funded by Russian Foundation for Basic Research (project number 19-34-60020) and Ministry of Science and Higher Education of the Russian Federation (project FSRZ-2020-0014). J.A. was funded by research grants 20-05840Y of the Czech Science Foundation, INTER-EXCELLENCE LTAUSA19137 provided by Czech Ministry of Education, Youth and Sports, and long-term research development project No. RVO 67985939 of the Czech Academy of Sciences.

References

- Abdullah, H., Skidmore, A.K., Darvishzadeh, R. & Heurich, M. (2019) Sentinel-2 accurately maps green-attack stage of European spruce bark beetle (*Ips typographus*, L.) compared with Landsat-8. *Remote Sensing in Ecology and Conservation*, **5**, 87–106. <https://doi.org/10.1002/rse2.93>
- Alhindhi, T.J., Kalra, S., Ng, K.H., Afrin, A. & Tizhoosh, H.R. (2018) Comparing LBP, HOG and deep features for classification of histopathology images. arXiv:1805.05837v1.
- Altman, J., Ukhvatkina, O., Omelko, A., Macek, M., Plener, T., Plener, T. et al. (2018) Poleward migration of the destructive effects of tropical cyclones during the 20th century. *PNAS*, **115**, 11543–11548. <https://doi.org/10.1073/pnas.1808979115>
- Boykov, Y., Veksler, O. & Zabih, R. (2001) Fast approximate energy minimization via graph cuts. *IEEE Transactions on Pattern Analysis*, **23**, 1222–1239. <https://doi.org/10.1109/34.969114>
- Breiman, L. (2001) Random forests. *Machine Learning*, **45**, 5–32. <https://doi.org/10.1023/A:1010933404324>
- Chen, L., Papandreou, G., Schroff, F. & Adam, H. (2017) Rethinking atrous convolution for semantic image segmentation. arXiv:1706.05587.
- Chollet, F., Rahman, F., Lee, T., de Marmiesse, G., Zabluda, O., Pumperla, M. et al. (2015) Keras. <https://github.com/fchollet/keras>
- Cortes, C. & Vapnik, V. (1995) Support-vector networks. *Machine Learning*, **20**, 273–297. <https://doi.org/10.1007/BF00994018>
- Dale, V., Joyce, L., McNulty, S., Neilson, R., Ayres, M., Flannigan, M.D. et al. (2001) Climate change and forest disturbances: climate change can affect forests by altering the frequency, intensity, duration, and timing of fire, drought, introduced species, insect and pathogen outbreaks, hurricanes, windstorms, ice storms, or landslides. *BioScience*, **51**, 723–734.
- de Groot, M., Ogris, N. & Kobler, A. (2018) The effects of a large-scale ice storm event on the drivers of bark beetle outbreaks and associated management practices. *Forest Ecology and Management*, **408**, 195–201. <https://doi.org/10.1016/j.foreco.2017.10.035>
- Dennison, P.E., Brunelle, A.R. & Carter, V.A. (2010) Assessing canopy mortality during a mountain pine beetle outbreak using GeoEye-1 high spatial resolution satellite data. *Remote Sensing of Environment*, **114**, 2431–2435. <https://doi.org/10.1016/j.rse.2010.05.018>
- Dhanachandra, N., Manglem, K. & Chanu, Y.J. (2015) Image segmentation using K-means clustering algorithm and subtractive clustering algorithm. *Procedia Computer Science*, **54**, 764–771. <https://doi.org/10.1016/j.procs.2015.06.090>
- Dixon, R.K., Solomon, A.M., Brown, S., Houghton, R.A., Trexier, M.C. & Wisniewski, J. (1994) Carbon pools and flux of global forest ecosystems. *Science*, **263**, 185–190. <https://doi.org/10.1126/science.263.5144.185>
- Duarte, D., Nex, F., Kerle, N. & Vosselman, G. (2018) Multi-resolution feature fusion for image classification of building damages with convolutional neural networks. *Remote Sensing*, **10**, 1636. <https://doi.org/10.3390/rs10101636>
- Einzmann, K., Immitzer, M., Böck, S., Bauer, O., Schmitt, A. & Atzberger, C. (2017) Windthrow detection in European forests with very high-resolution optical data. *Forests*, **8**, 21. <https://doi.org/10.3390/f8010021>
- Freund, Y. & Schapire, R.E. (1997) A decision-theoretic generalization of on-line learning and an application to boosting. *Journal of Computer and System Sciences*, **55**, 119–139. <https://doi.org/10.1006/jcss.1997.1504>
- Hamdi, Z.M., Brandmeier, M. & Straub, C. (2019) Forest damage assessment using deep learning on high resolution remote sensing data. *Remote Sensing*, **11**, 1976. <https://doi.org/10.3390/rs11171976>
- Haralick, R.M., Shanmugam, K. & Dinstein, I. (1973) Textural features for image classification. *IEEE Transactions on Systems, Man, and Cybernetics*, **6**, 610–621. <https://doi.org/10.1109/TSMC.1973.4309314>
- Havašová, M., Ferencík, J. & Jakub, R. (2017) Interactions between windthrow, bark beetles and forest management in the Tatra national parks. *Forest Ecology and Management*, **391**, 349–361. <https://doi.org/10.1016/j.foreco.2017.01.009>
- Huberty, C.J. (1975) Discriminant analysis. *Review of Educational Research*, **45**, 543–598. <https://doi.org/10.3102/00346543045004543>

- Humeau-Heurtier, A. (2019) Texture feature extraction methods: a Survey. *IEEE Access*, **7**, 8975–9000. <https://doi.org/10.1109/ACCESS.2018.2890743>
- Junttila, S., Holopainen, M., Vastaranta, M., Lyytikäinen-Saarenmaa, P., Kaartinen, H. et al. (2019) The potential of dual-wavelength terrestrial lidar in early detection of *Ips typographus* (L.) infestation – Leaf water content as a proxy. *Remote Sensing of Environment*, **231**, 111264. <https://doi.org/10.1016/j.rse.2019.111264>
- Kass, M., Witkin, A. & Terzopoulos, D. (1988) Snakes: active contour models. *International Journal of Computer Vision*, **1**, 321–331. <https://doi.org/10.1007/BF00133570>
- Kattenborn, T., Eichel, J. & Fassnacht, F.E. (2019) Convolutional Neural Networks enable efficient, accurate and fine-grained segmentation of plant species and communities from high-resolution UAV imagery. *Scientific Reports*, **9**, 17656. <https://doi.org/10.1038/s41598-019-53797-9>
- Kattenborn, T., Eichel, J., Wiser, S., Burrows, L., Fassnacht, F.E. & Schmidlein, S. (2020) Convolutional Neural Networks accurately predict cover fractions of plant species and communities in Unmanned Aerial Vehicle imagery. *Remote Sensing in Ecology and Conservation*. <https://doi.org/10.1002/rse2.146>
- Kingma, D.P. & Ba, J. (2014) Adam: a method for stochastic optimization. [arXiv:1412.6980](https://arxiv.org/abs/1412.6980).
- Kislov, D.E. & Korznikov, K.A. (2020) Automatic windthrow detection using very-high resolution satellite imagery and deep learning. *Remote Sensing*, **12**, 1145. <https://doi.org/10.3390/rs12071145>.
- Krizhevsky, A., Sutskever, I. & Hinton, G.E. (2017) Imagenet classification with deep convolutional neural networks. *Communications of the ACM*, **60**, 84–90. <https://doi.org/10.1145/3065386>
- Lee, S.Y., Tama, B.A., Moon, S.J. & Lee, S. (2019) Steel surface defect diagnostics using deep convolutional neural network and class activation map. *Applied Sciences*, **9**, 5449. <https://doi.org/10.3390/app9245449>
- Liang, J., Crowther, T.W., Picard, N., Wiser, S., Zhou, M., Alberti, G. et al. (2016) Positive biodiversity-productivity relationship predominant in global forests. *Science*, **354**, aaf8957. <https://doi.org/10.1126/science.aaf8957>
- Ma, L., Liu, Y., Zhang, X., Ye, Y., Yin, G. & Johnson, B.A. (2019) Deep learning in remote sensing applications: a meta-analysis and review. *ISPRS Journal of Photogrammetry and Remote Sensing*, **152**, 166–177. <https://doi.org/10.1016/j.isprsjprs.2019.04.015>
- Mannor, S., Peleg, D. & Rubinstein, R. (2005) The cross entropy method for classification. In S. Dzeroski, L. De Raedt & S. Wrobel (Eds.), *ICML '05: proceedings of the 22nd international conference on Machine learning*. New York, NY, United States: Association for Computing Machinery, pp. 561–568. <https://doi.org/10.1145/1102351.1102422>
- Mazza, A., Sica, F., Rizzoli, P. & Scarpa, G. (2019) TanDEM-X forest mapping using convolutional neural networks. *Remote Sensing*, **11**, 2980. <https://doi.org/10.3390/rs11242980>
- McConnell, R.K. (1986) *Method of and apparatus for pattern recognition*. <https://www.osti.gov/biblio/6007283-method-apparatus-pattern-recognition>
- Mesner, N. & Oštirb, K. (2014) Investigating the impact of spatial and spectral resolution of satellite images on segmentation quality. *Journal of Applied Remote Sensing*, **8**, 083696. <https://doi.org/10.1117/1.JRS.8.083696>
- Millar, C.I. & Stephenson, N.L. (2015) Temperate forest health in an era of emerging megadisturbance. *Science*, **349**, 823–826. <https://doi.org/10.1126/science.aaa9933>
- Minaee, S., Boykov, Y., Porikli, F., Plaza, A., Kehtarnavaz, N. & Terzopoulos, D. (2020) *Image segmentation using deep learning: a survey*. [arXiv:2001.05566](https://arxiv.org/abs/2001.05566)
- Moré, J.J. (1978) The Levenberg-Marquardt algorithm: implementation and theory. In G.A. Watson (Ed.), *Numerical analysis. Lecture notes in mathematics*, vol. **630**. Berlin, Heidelberg: Springer, pp. 105–116. <https://doi.org/10.1007/BFb0067700>
- Nock, R. & Nielsen, F. (2004) Statistical region merging. *IEEE Transactions on Pattern Analysis and Machine Intelligence*, **26**, 1452–1458. <https://doi.org/10.1109/TPAMI.2004.110>
- Olsson, P.-O., Lindström, J. & Eklundh, L. (2016) Near real-time monitoring of insect induced defoliation in subalpine birch forests with MODIS derived NDVI near real-time monitoring. *Remote Sensing of Environment*, **181**, 42–53. <https://doi.org/10.1016/j.rse.2016.03.040>
- Otsu, N. (1979) A threshold selection method from gray-level histograms. *IEEE Transactions on Systems, Man, and Cybernetics*, **9**, 62–66. <https://doi.org/10.1109/TSMC.1979.4310076>
- Paoletti, M., Haut, J., Plaza, J. & Plaza, A. (2019) Deep learning classifiers for hyperspectral imaging: a review. *ISPRS Journal of Photogrammetry and Remote Sensing*, **158**, 279–317. <https://doi.org/10.1016/j.isprsjprs.2019.09.006>
- Pedregosa, F., Varoquaux, G., Gramfort, A., Michel, V., Thirion, B., Grisel, O. et al. (2011) Scikit-learn: machine learning in python. *Journal of Machine Learning Research*, **12**, 2825–2830. <https://www.jmlr.org/papers/volume12/rigollet11a/rigollet11a.pdf>
- Plath, N., Toussaint, M. & Nakajima, S. (2009) Multi-class image segmentation using conditional random fields and global classification. In A. Danyluk, L. Bottou & M. Littman (Eds.), *ICML '09: proceedings of the 26th Annual International Conference on Machine Learning*. New York, NY, United States: Association for Computing Machinery, pp. 817–824. <https://doi.org/10.1145/1553374.1553479>
- Potapov, P., Hansen, M.C., Kommareddy, I., Kommareddy, A., Turubanova, S., Pickens, A. et al. (2020) Landsat analysis ready data for global land cover and land cover change mapping. *Remote Sensing*, **12**, 426. <https://doi.org/10.3390/rs12030426>.

- Quine, C., Coutts, M., Gardiner, B. & Pyatt, G. (1995) In: *Forests and wind: management to minimise damage*. Forestry commission bulletin, **144**. London: HMSO. <https://www.forestryresearch.gov.uk/documents/6581/FCBU114.pdf>
- Rezatofighi, H., Tsoi, N., Gwak, J., Sadeghian, A., Reid, I. & Savarese, S. (2019) *Generalized Intersection over Union: a metric and a loss for bounding box regression*. arXiv:1902.09630.
- Ronneberger, O., Fischer, P. & Brox, T. (2015) U-Net: convolutional networks for biomedical image segmentation. In N. Navab, J. Hornegger, W.M. Wells & A.F. Frangi (Eds.), *MICCAI 2015: medical image computing and computer-assisted intervention – MICCAI 2015*. Cham: Springer, (pp. 234–241). https://doi.org/10.1007/978-3-319-24574-4_28
- Safonova, A., Tabik, S., Alcaraz-Segura, D., Rubtsov, A., Maglinets, Y. & Herrera, F. (2019) Detection of fir trees (*Abies sibirica*) damaged by the bark beetle in unmanned aerial vehicle images with deep learning. *Remote Sensing*, **11**, 643. <https://doi.org/10.3390/rs11060643>
- Seidl, R., Thom, D., Kautz, D., Martin-Benito, D., Peltoniemi, M., Vacchiano, G. et al. (2017) Forest disturbances under climate change. *Nature Climate Change*, **7**, 395–402. <https://doi.org/10.1038/nclimate3303>
- Senf, C., Pfugmacher, D., Hostert, P. & Seidl, R. (2017) Using Landsat time series for characterizing forest disturbance dynamics in the coupled human and natural systems of Central Europe. *ISPRS Journal of Photogrammetry and Remote Sensing*, **130**, 453–463. <https://doi.org/10.1016/j.isprsjprs.2017.07.004>
- Shorten, C. & Khoshgoftaar, T. (2019) A survey on image data augmentation for deep learning. *Journal of Big Data*, **6**, 60. <https://doi.org/10.1186/s40537-019-0197-0>
- Sommerfeld, A., Senf, C., Burna, B., D'Amato, A., Després, T., Díaz-Hormazábal, I. et al. (2018) Patterns and drivers of recent disturbances across the temperate forest biome. *Nature Communications*, **9**, 4355. <https://doi.org/10.1038/s41467-018-06788-9>
- Starck, J., Elad, M. & Donoho, D.L. (2005) Image decomposition via the combination of sparse representations and a variational approach. *IEEE Transactions on Image Processing*, **14**, 1570–1582. <https://doi.org/10.1109/TIP.2005.852206>
- Sulla-Menashe, D., Kennedy, R.E., Yang, Z., Braaten, J., Krankina, O.N. & Friedl, M.A. (2014) Detecting forest disturbance in the Pacific Northwest from MODIS time series using temporal segmentation. *Remote Sensing of Environment*, **151**, 114–123. <https://doi.org/10.1016/j.rse.2013.07.042>
- Sylvain, J.-D., Drolet, G. & Brown, N. (2019) Mapping dead forest cover using a deep convolutional neural network and digital aerial photography. *ISPRS Journal of Photogrammetry and Remote Sensing*, **156**, 14–26. <https://doi.org/10.1016/j.isprsjprs.2019.07.010>
- Vlasov, S. (1959) *Forests of Sakhalin Island*. (In Russian: Lesa Sakhalina). Sakhalinskoe knizhnoe izdatelstvo, Yuzhno-Sakhalinsk.
- Wagner, F.H., Sanchez, A., Tarabalka, Y., Lotte, R.G., Ferreira, M.P., Aidar, M.P.M. et al. (2019) Using the U-net convolutional network to map forest types and disturbance in the Atlantic rainforest with very high resolution images. *Remote Sensing in Ecology and Conservation*, **5**, 360–375. <https://doi.org/10.1002/rse2.111>
- Webster, P., Holland, G., Curry, J. & Chang, H.-R. (2005) Changes in tropical cyclone number, duration, and intensity in a warming environment. *Science*, **309**, 1844–1846. <https://doi.org/10.1126/science.1116448>
- Yuan, Q., Shen, H., Li, T., Li, Z., Li, S., Jiang, Y. et al. (2020) Deep learning in environmental remote sensing: achievements and challenges. *Remote Sensing of Environment*, **241**, 111716. <https://doi.org/10.1016/j.rse.2020.111716>
- Zhang, H. (2004) The optimality of naive Bayes. In V. Barr & Z. Markov (Eds.) *Proceedings of the Seventeenth International Florida Artificial Intelligence Research Society Conference*, pp. 562–568. Menlo Park, California: The AAAI Press. <https://www.aaai.org/Papers/FLAIRS/2004/Flairs04-097.pdf>